Evaluating efficiency and robustness in cilia design

Hanliang Guo and Eva Kanso*

Department of Aerospace and Mechanical Engineering, University of Southern California, Los Angeles, California 90089, USA

(Received 21 December 2015; revised manuscript received 24 February 2016; published 21 March 2016)

Motile cilia are used by many eukaryotic cells to transport flow. Cilia-driven flows are important to many physiological functions, yet a deep understanding of the interplay between the mechanical structure of cilia and their physiological functions in healthy and diseased conditions remains elusive. To develop such an understanding, one needs a quantitative framework to assess cilia performance and robustness when subject to perturbations in the cilia apparatus. Here we link cilia design (beating patterns) to function (flow transport) in the context of experimentally and theoretically derived cilia models. We particularly examine the optimality and robustness of cilia design. Optimality refers to efficiency of flow transport, while robustness is defined as low sensitivity to variations in the design parameters. We find that suboptimal designs can be more robust than optimal ones. That is, designing for the most efficient cilium does not guarantee robustness. These findings have significant implications on the understanding of cilia design in artificial and biological systems.

DOI: 10.1103/PhysRevE.93.033119

I. INTRODUCTION

Cilia are hairlike structures, typically tens of micrometers in length, that protrude from the surface of eukaryotic cells. They can be found in many aquatic and terrestrial species from the unicellular protozoan *Paramecium* to humans. In mammals, cilia are present on many cells in the body, either in large groups on a single cell, as in the case of motile cilia, or as solitary structures, as in the case of primary and nodal cilia [1]. Motile cilia, the focus of this work, are found on the epithelial cells of the trachea [2–4], ependymal cells in the brain [5,6], and cells lining the oviduct and epididymis of the reproductive tracts [7]. They normally beat in an orchestrated fashion resulting in fluid movement and cell transport [8]. Great advances have been made in demonstrating the importance of ciliary transport to many physiological functions [9,10] and in unraveling the underlying fluid-structure interactions at the cilia scale [11–15]. However, a deep understanding of the interplay between the mechanical structure of cilia and their physiological functions and how ciliary dysfunction can lead to severe disease and developmental pathologies remains elusive.

It is therefore important to apply quantitative measures that link cilia mechanics (e.g., cilia beating patterns) to function (e.g., flow transport) in both healthy and diseased states [16,17]. The lack of such standardized measures is in part due to the use of disparate research approaches in the biological and physical sciences. In health-related research, a traditional approach is to use *in vitro* ciliated cell cultures, from which the fundamental structure-function relationships are inferred. However, the clinical use of such *in vitro* cell cultures has been mostly qualitative. In biofluid mechanics research, an increasingly popular approach consists of computing the ideal kinematics for a single function, such as optimal fluid transport in cilia acting both individually [18] and collectively [19]. This optimization approach requires a sophisticated mathematical and computational apparatus to arrive at the optimal cilia kinematics. The optimal result provides valuable insights into ciliary design, but fails to explain, let alone evaluate, the variation in cilia kinematics and how deviations from such kinematics affect cilia function. Here we posit that robustness under perturbations to cilia kinematics, whether due to environmental or structural causes, is of paramount importance for healthy cilia function. As such, lack of robustness can be linked to cilia dysfunction and disease. We therefore present an alternative approach that emphasizes the design principles amenable to a given function (flow transport) and the robustness of such a function under variations in the cilia design parameters.

The beating cycle of a cilium typically consists of two phases: an effective stroke aimed at generating flow followed by a recovery stroke during which the cilium returns to its initial position. During the effective stroke, the cilium moves in an almost straight configuration in a plane normal to the cell surface, while in the recovery stroke, it bends parallel to the cell surface while exhibiting large curvatures and possibly moving out of the normal plane. The details of the cilia beat kinematics depend on the cell type, but the exact physical and/or biological mechanisms that select or constrain these kinematics are not well understood. We posit that optimality is not the main mechanism driving this selection. This conviction is in part based on a recent comparative study of the performance of two cilia beating patterns taken from two experimental systems, namely, cilia from a swimming micro-organism and rabbit tracheal cilia. In the first system, cilia are used for swimming, while in the second, they are used for fluid transport. If cilia performance were hydrodynamically optimal, one would expect the transport-specific cilia to outperform the swimming-specific cilia in fluid transport and vice versa. However, by comparing the two types of cilia, we found the cilia beating pattern taken from the swimming system to be consistently superior to the other in three different hydrodynamic performance metrics. These findings imply that cilia beating kinematics need not be optimal hydrodynamically [20]. Further, in mammalian cells, cilia beating motion takes a minimal fraction of the metabolic budget of the body. It is therefore unlikely, from the perspective

*kanso@usc.edu

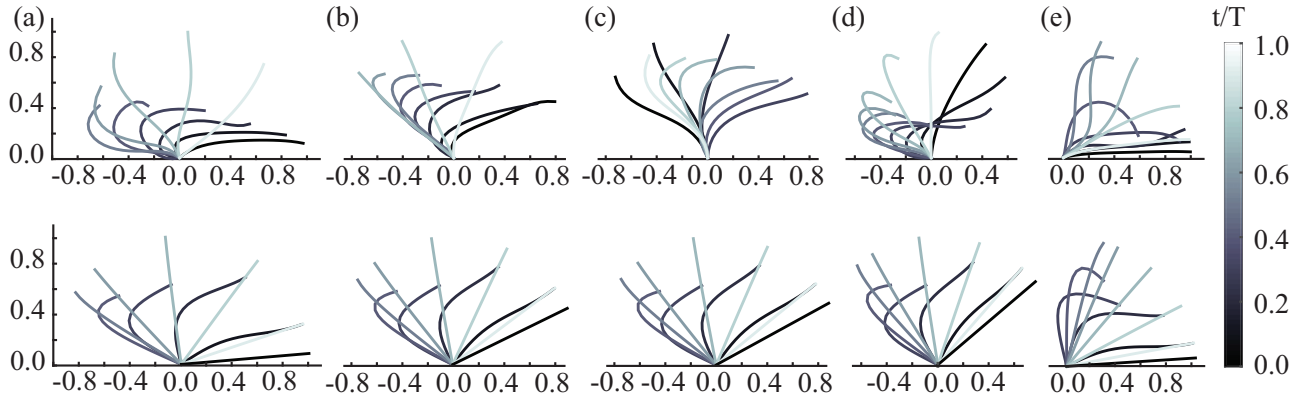

FIG. 1. The top row shows cilia beating patterns reconstructed from experimental data extracted from Sleigh [23] and Fulford and Blake [2] for (a) *Didinium*, (b) *Paramecium*, (c) rabbit tracheal cilia, (d) *Sabellaria* gill, and (e) *Opalina*. The bottom row shows the mathematical model presented in this paper where the values of λ_0 and α_0 are extracted from the experimental images in the top row.

of evolutionary biology, that the energetic cost associated with the beating of a cilium has posed a major selective pressure on its beat kinematics. In contrast, the energetic cost associated with locomotion consumes a significant portion of the metabolic budget in almost all motile organisms [21], thus justifying the need for an optimal or quasioptimal gait. This is also true in cilia-driven locomotion such as in the protozoan *Paramecium* [22]. The *Paramecium* uses more than half its total energy consumption for swimming, while its hydrodynamic swimming efficiency is estimated to be as low as 0.77%. However, it is important to distinguish between optimizing the cilium kinematics and optimizing the swimming gait. The latter involves, in addition to the cilium kinematics, the coordination between multiple cilia and different cilia types as well as their distribution on the underlying surface and the geometric properties of that surface.

In this study we examine the beating kinematics of individual cilia in relation to their function in fluid transport. We propose three reduced design parameters that capture the salient kinematic features of motile cilia, namely, the leaning angle in the direction of the effective stroke, the beating amplitude of the effective stroke, and the out-of-plane angle. We present a straightforward approach for extracting these design parameters from any cilia beating pattern, including those obtained experimentally from high-speed image sequences. We then present a mathematical family of cilialike kinematics that can be constructed for any combination of design parameters.

We validate this choice of generic cilialike kinematics by comparing it to experimentally derived cilia kinematics before we use it to investigate questions of optimality and robustness of cilia design. Optimality here is defined in terms of the efficiency of flow transport, while robustness refers to a lack of sensitivity in transport efficiency to variations in the design parameters. We find that suboptimal kinematics are more robust than optimal kinematics. That is, there is an interplay between optimality and robustness in cilia design. Our findings provide a quantitative framework for investigating cilia performance under various operating conditions and thus have significant implications in the understanding of cilia design in artificial and biological systems.

II. MODEL AND METHOD

We consider a cilium whose base point is chosen to coincide with the origin of properly chosen Cartesian coordinates (x,y,z). The length of the cilium is l. The cilium beats periodically in the half infinite domain $y > 0$ with frequency ω and period $T = 2\pi/\omega$.

The beating motion of the cilium is represented by $\mathbf{x}_c(s,t) \equiv (x_c(s,t), y_c(s,t), z_c(s,t))$, where s is the arc length along the cilium's centerline from its base $(0 < s < l)$ and t is time $(0 < t < T)$. To describe the cilia beating kinematics from experimental observation of cilia beat patterns [2,23], we write each component of $\mathbf{x}_c(s,t)$ using a Taylor series expansion in s and Fourier series expansion in t. We then calculate the series coefficients that best fit the experimental data [2,23] subject to the constraint that the total length of the cilium is conserved (see Fig. 1). Here, for consistency and without loss of generality, we consider the effective stroke direction to be pointing in the positive x direction. It is clear from Fig. 1 that the details of the cilia beating kinematics vary depending on the cell type, but qualitatively they all follow the same trend. Further, all these examples correspond to planar cilia kinematics. Based on the original planar images in Refs. [2,23], it is relatively straightforward to assess whether the bending kinematics is planar by comparing the projected cilium length in the experimental image sequence of the beat cycle to the absolute cilium length [23]. In each of the cases presented here, we found little change in the cilium's overall length over one beating cycle (with standard deviation about 3%), indicating that the cilium bending motion is mostly two dimensional. Note that in the cases when the cilia kinematics is nonplanar, it is very difficult to uniquely reconstruct the out-of-plane motion from planar images. For this reason, we only reconstructed planar kinematics in Fig. 1.

In order to facilitate the comparison between the beating kinematics of various cilia type, it is useful to describe the cilia beating patterns mathematically using a small number of parameters. Concise mathematical descriptions date back to Taylor's swimming sheet [24], albeit for modeling symmetric beating motion. Asymmetric beating patterns were later described using various approaches, including the biased baseline mechanisms [25], the Taylor and Fourier series

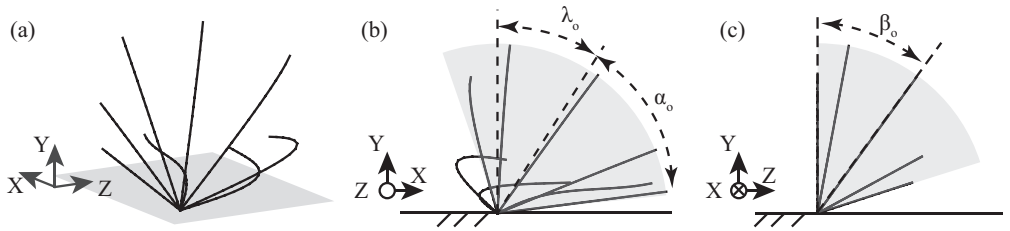

FIG. 2. Reduced cilia design parameters λ_0, α_0, and β_0. (a) Three-dimensional beating pattern of the cilium. (b) Projection onto the plane of the effective stroke showing the leaning angle λ_0 and beating amplitude α_0. (c) Projection onto the plane normal to the effective stroke showing the out-of-plane swinging angle β_0.

expansions [2] employed above, and more recently, efficient polynomial expansions [26] and curvature-based Fourier series expansions [27]. These methods can reconstruct the beating patterns from given experimental data, but often require sophisticated machinery and a large number of parameters. Here we introduce three reduced cilia design parameters that can be used to reconstruct any beating patterns in three dimensions: the leaning angle λ_0, the beating amplitude α_0, and the swinging angle β_0, as shown in Fig. 2. To define these parameters, we first let λ be the angle between the straight line pointing from the cilium base to the cilium tip and the (y,z) plane and β be the angle between the plane containing the curved cilium and the (x,y) plane. Positive λ are taken to be counterclockwise about the positive z axis, whereas positive β are measured clockwise about the positive x axis. Basically, λ describes the amount by which the cilium is leaning in the direction of the effective stroke, while β describes the amount by which the cilium leans away from the plane of the effective stroke in the positive z axis. The three design parameters λ_0, α_0, and β_0 can then be defined as follows:

$$\begin{aligned}\lambda_0 &= \frac{1}{2}\Big[\max_{0\leqslant t<T}(\lambda) + \min_{0\leqslant t<T}(\lambda)\Big],\\ \alpha_0 &= \frac{1}{2}\Big[\max_{0\leqslant t<T}(\lambda) - \min_{0\leqslant t<T}(\lambda)\Big],\\ \beta_0 &= \frac{1}{2}\Big[\max_{0\leqslant t<T}(\beta) + \min_{0\leqslant t<T}(\beta)\Big].\end{aligned} \tag{1}$$

For the examples reported in Fig. 1, β and β_0 are identically zero. These three parameters capture the salient features of the actual beating patterns but not all their details. The main reason we choose these parameters is that they are easy to access from experimental images and they are amenable to a low-order mathematical representation of asymmetric cilia beating patterns as discussed next.

We now introduce a mathematical family of functions that emulates cilia beating kinematics. This mathematical family can be viewed as a blueprint for generating cilia beating kinematics that satisfies given cilia design parameters (λ_0, α_0, and β_0). Basically, we use a sinusoidal function to describe the shape of the cilium at different times in local Cartesian coordinates; we then rotate the shape according to the design parameters λ_0, α_0, and β_0 to generate cilialike kinematics. To this end, we set

$$\zeta(\xi,t) = lA(t)\sin\left(\frac{3\pi}{2}\frac{\xi}{l}\right), \quad A(t) = 1-\cos\left(\pi\frac{t}{T}\right). \tag{2}$$

Here (ξ,ζ) are local Cartesian coordinates that must satisfy the constraint that the total length of the cilium is constant for all time t. Namely, one has $ds = \sqrt{(d\xi)^2+(d\zeta)^2}$, which yields $\int_0^l ds = \int_0^l d\xi\sqrt{1+(d\zeta/d\xi)^2} = l$. By virtue of the implicit function theorem, one can use this equality together with (2) to write $\xi(s,t)$ and $\zeta(s,t)$ as functions of arc length and time. Figure 3(a) is a depiction of the kinematics obtained from these generating functions. The wave number $3\pi/2$ is chosen so that the cilium does not exhibit both positive and negative curvatures at any given time, consistent with experimental observation of cilia beating patterns (see Fig. 1 and analysis in Ref. [23]). The time-dependent wave amplitude $A(t)$ is chosen so that the cilium is less curved in the effective stroke ($0.5T < t < T$) than in the recovery stroke ($0 < t < 0.5T$). Note that one can expand this representation in terms of a second-order Taylor expansion in s, given that no inflection points in the cilium shape are allowed, and a Fourier series expansions in

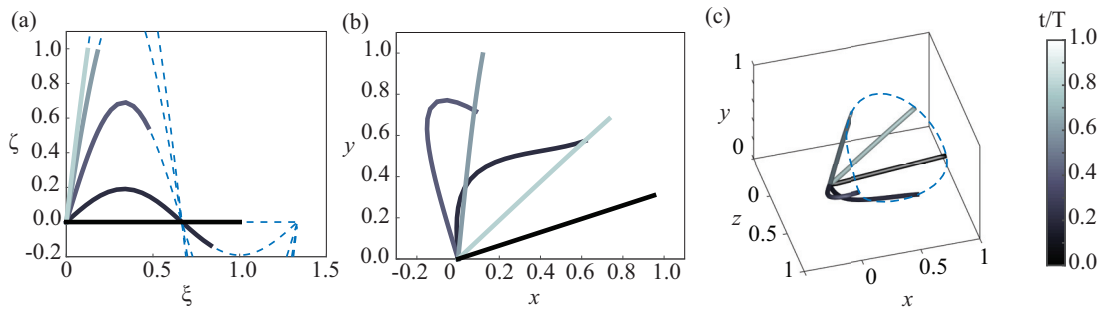

FIG. 3. Generic cilialike kinematics. (a) Shapes of the strokes at select times are constructed from truncated sinusoidal functions that ensure conservation of the total length of the cilium. (b) Planar beating patterns at select times. (c) Beating patterns at select phases in three-dimensional space. The parameter values in all panels are $\lambda_0 = 0.2\pi$, $\alpha_0 = 0.2\pi$, and $\beta_0 = 0.2\pi$.

time. The coefficients of these expansions are omitted here for brevity.

Cilialike kinematics with desired values of λ_0, α_0, and β_0 can be constructed using the blueprint $(\xi(s,t),\zeta(s,t))$ as follows. We first write the instantaneous leaning angle $\lambda(t)$ and swinging angle $\beta(t)$ as explicit functions of time

$$\lambda(t) = \lambda_0 + \alpha_0 \cos\left(2\pi \frac{t}{T}\right),$$
$$\beta(t) = \beta_0\left[1 + \sin\left(2\pi \frac{t}{T}\right)\right]. \tag{3}$$

We then rotate (ξ,ζ) about the z axis by an angle $\lambda - \arctan(\xi(l,t)/\zeta(l,t))$ to produce the cilium bending motion in the (x,y) plane [see Fig. 3(b)]. To make the cilium swing out of the vertical plane, we perform a second rotation about the x axis by the angle β [see Fig. 3(c)]. At the end of these two rotations, one obtains cilialike kinematics $(x_c(s,t),y_c(s,t),z_c(s,t))$ that satisfy the desired design parameters λ_0, α_0, and β_0. This family of beating kinematics qualitatively resembles the beating patterns of biological cilia in that the effective stroke is straight and perpendicular to the base surface, while the recovery stroke is curly and close to the base surface. The beating kinematics, by construction, spend an equal amount of time in effective and recovery strokes. The hydrodynamic performance, however, is independent of time because the flow in the Stokes regime is essentially a geometric problem.

We use l and T to scale length and time, respectively. All variables are thereafter nondimensional. The fluid motion is governed by the nondimensional Stokes equation and incompressibility condition at zero Reynolds number

$$-\nabla p + \mu\nabla^2\mathbf{u} = \mathbf{0}, \quad \nabla\cdot\mathbf{u} = 0, \tag{4}$$

where p is the pressure field, μ is the dimensionless viscosity, and $\mathbf{u}$ is the fluid velocity field. The boundary condition at the cilium and base surface is a no-slip condition

$$\mathbf{u}|_{\text{boundary}} = \begin{cases} \mathbf{u}_c & \text{at the cilium} \\ \mathbf{0} & \text{at the base surface,} \end{cases} \tag{5}$$

where $\mathbf{u}_c$ is the prescribed velocity of the cilium, based on the kinematics reconstructed from either experimental images or the mathematical formulation.

We solve (4) and (5) numerically using the regularized Stokeslet method [28]. The cilium is approximated by a distribution of regularized Stokeslets along its centerline, together with an image distribution to impose the no-slip boundary conditions at the base surface [29]. The velocity at any point $\mathbf{x}$ induced by a regularized Stokeslet of strength $\mathbf{f}_i$ located at $\mathbf{x}_i$ and its images can be written as $\mathbf{G}_s(\mathbf{x}-\mathbf{x}_i)\cdot\mathbf{f}_i$, where $\mathbf{G}_s$ is the regularized Green's tensor-valued function given by Ainley *et al.* [29]. The total velocity generated by all regularized Stokeslets is then

$$\mathbf{u}(\mathbf{x}) = \sum_{i=1}^{n} \mathbf{G}_s(\mathbf{x}-\mathbf{x}_i)\cdot\mathbf{f}_i, \tag{6}$$

where n is the total number of regularized Stokeslets. The expression in Eq. (6) is substituted into (5) to obtain a system of equations that can be used to compute the strengths $\mathbf{f}_i$ of the regularized Stokeslets. Once $\mathbf{f}_i$ are known, the flow field can be reconstructed everywhere.

Let Q_x and Q_z denote the flow transported by the cilium in the x and z directions, respectively. One has (see [15,30,31] for more details)

$$Q_x = \frac{1}{\mu\pi}\int_0^l (\mathbf{f}_i\cdot\mathbf{e}_x) y\, ds, \quad Q_z = \frac{1}{\mu\pi}\int_0^l (\mathbf{f}_i\cdot\mathbf{e}_z) y\, ds, \tag{7}$$

where $\mathbf{e}_x$ and $\mathbf{e}_z$ are the unit vectors in the x and z directions. These expressions are based on the fact that the net flux generated by a Stokeslet over an infinite plane is directly proportional to the height of the Stokeslet above the plane [30]. Now consider the time average of the flow rates per cycle: $\langle Q_x\rangle = \frac{1}{T}\int_0^T Q_x dt$ and $\langle Q_z\rangle = \frac{1}{T}\int_0^T Q_z dt$. The total average flow rate is $\langle Q\rangle = \sqrt{\langle Q_x\rangle^2 + \langle Q_z\rangle^2}$.

To compute the internal power spent by the cilium during the beating cycle, we consider each cilium to be an inextensible elastic filament and adopt the Kirchhoff equations of motion for a rod [18,20]

$$\frac{\partial\mathbf{N}}{\partial s} - \mathbf{f} = 0, \quad \frac{\partial\mathbf{M}}{\partial s} + \mathbf{t}\times\mathbf{N} + \mathbf{q} = 0. \tag{8}$$

Here $\mathbf{N}(s,t)$ and $\mathbf{M}(s,t)$ are the internal tension and elastic moment, respectively, $\mathbf{f}(s,t)$ is the force exerted by the cilium on the surrounding fluid, $\mathbf{t} = \partial\mathbf{x}_c/\partial s$ is the unit tangent to the cilium, and $\mathbf{q}(s,t)$ is the internally generated moment per unit length. The internal bending moment $\mathbf{q}$ resembles the moments generated by the cilium internal motors.

The force distribution $\mathbf{f}$ is computed by dividing the local Stokeslet strength $\mathbf{f}_i$ by the distance between neighboring Stokeslets along the cilium. We assume a linear constitutive relation between the elastic moment $\mathbf{M}$ along the cilium and the deformation [18,20]. Namely, we set $\mathbf{M} = B\mathbf{D}$, where B is the bending rigidity and $\mathbf{D} = \mathbf{t}\times(\partial\mathbf{t}/\partial s)$ is the Darboux vector. Substituting $\mathbf{M} = B\mathbf{D}$ into (8), one gets the expression of the internal moments generated along the cilium

$$\mathbf{q} = B\frac{\partial^2\mathbf{t}}{\partial s^2}\times\mathbf{t} + \mathbf{t}\times\int_s^l \mathbf{f}(\tilde{s},t)d\tilde{s}. \tag{9}$$

The average power $\langle P\rangle$ expended internally by the cilium to transport is equal to the power consumed by the internal moments $\mathbf{q}$,

$$\langle P\rangle = \left\langle \int_0^l \max(0,\mathbf{q}\cdot\boldsymbol{\Omega})ds \right\rangle, \tag{10}$$

where $\boldsymbol{\Omega} = \|\dot{\mathbf{t}}(s)\|\frac{\mathbf{t}\times\dot{\mathbf{t}}}{\|\mathbf{t}\times\dot{\mathbf{t}}\|}$ is the angular velocity vector, with the overdot denoting the time derivative. Here, only the positive works are accounted for, i.e., the cilium does not harvest energy from the environment [18,32]. This implies that the mean power spent by the cilium's internal moments is larger than the power given to the fluid. Finally, we define a dimensionless transport efficiency

$$\eta = \mu l^{-3}\frac{\langle Q\rangle^2}{\langle P\rangle}, \tag{11}$$

which is consistent with that employed by Osterman and Vilfan [19] and Eloy and Lauga [18].

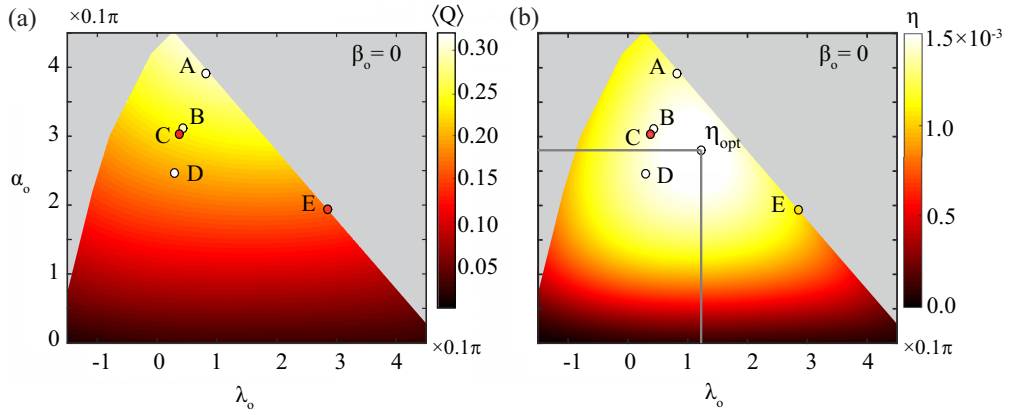

FIG. 4. Flow rate $\langle Q\rangle$ and efficiency η generated by the generic cilia model with $\beta_0 = 0$. Flow rates and the efficiencies of the cilia beating patterns reconstructed in Fig. 1 are plotted in circles at corresponding values of λ_0 and α_0. The color of the circle indicates the performance of these cilia using the color map of each panel. Deviations between the background color and the circle color indicate deviations in the performance of the generic model and actual cilia.

III. RESULTS

Our goal is to evaluate the hydrodynamic performance of the beating kinematics of individual cilia as a function of the three design parameters: the leaning angle λ_0, the beating amplitude α_0, and the out-of-plane swinging angle β_0. We use two evaluation metrics: the average flow rate $\langle Q\rangle$ and the efficiency η.

We discretize the cilium uniformly using 20 regularized Stokeslets. The regularization parameter is chosen to be 0.05, which yields a cilium length-to-radius ratio about 20. Each beating cycle is discretized into 100 time steps. By way of validation, we are able to reproduce the flow rates generated by embryonic primary cilia given by Smith *et al.* [31] with these discretization parameters.

We begin by considering planar cilia beat kinematics, for which $\beta_0 = 0$. We examine the performance of the cilium as a function of λ_0 and α_0. Namely, we vary λ_0 in the range from -0.15π to 0.45π and we vary α_0 from 0 to 0.45π using a step size of 0.01π. Combinations of parameters for which $\lambda_0 + \alpha_0 > 0.5\pi$ lead to prescribed cilium motion that penetrates the base surface. These combinations are considered unrealistic and not considered. Note that accurate information regarding the angular frequency and bending rigidity of cilia is sparse. Here, as well as in the rest of this section, we use the information available for the *Paramecium* as a proxy to obtain the right order of magnitude for the cilia angular frequency and bending rigidity. The typical length of the *Paramecium* cilia is about 10 μm, the typical angular frequency is about 200 rad s^{-1}, and the bending rigidity is estimated to be $B = 25$ pN μm^2 (see [18,33,34]). We thus use the characteristic length $l_c = 10$ μm, time $T_c = 2\pi/200 = 0.0314$ s, and viscosity $\mu_c = 10^{-3}$ Pa s. The nondimensional bending rigidity is then given by $B/\mu_c l_c^4 T_c^{-1} = 0.0785$. Note that more recent estimates of the bending rigidity predict higher values of B, e.g., [35]. However, the exact B value does not affect the main findings of this work, which focuses mainly on a comparative analysis of cilia performance under various design parameters.

The average flow rate $\langle Q\rangle$ and transport efficiency η for the admissible parameter values λ_0 and α_0 are shown in Fig. 4. It is clear from Fig. 4(a) that larger beating amplitude α_0 leads to larger average flow rate. Meanwhile, the leaning angle λ_0 has a small effect on the average flow rate. The beating patterns with small beating amplitude ($\alpha_0 \approx 0$) correspond to traveling waves somewhat similar to those observed in the flagella of sperm cells [33,36]. However, unlike the traveling waves in natural sperm cells, these waves are constrained such that the head and tip of the wave always lie at a constant direction from the substrate and the curvature of the wave has the same sign. If one were to use a flagellated sperm cell and adhere its head to a substrate such that its flagellum beats in such constraint traveling wave fashion, it would produce little flow.

The effect of α_0 and λ_0 on the transport efficiency η is depicted in Fig. 4(b). The beating pattern with $\lambda_0 = 0.12\pi$ and $\alpha_0 = 0.28\pi$ yields the highest transport efficiency 0.15%. Unlike its effect on $\langle Q\rangle$, a larger beating amplitude does not yield higher efficiency. This is because at higher α_0 the cilium will need to spend more power in its motion close to the base surface to overcome the zero velocity at that surface. The extra power needed to complete such beating cycles lowers the transport efficiency.

By way of validation of these generic cilialike kinematics, we compute the performance of the five beating patterns reconstructed from experimental data shown in Fig. 1. The leaning angles and beating amplitudes of these cilia are calculated according to (1). The flow rates and the transport efficiencies are then computed and the results are superimposed on Fig. 4 as colored circles in accord with their leaning angles and beating amplitudes. Clearly, the experimentally derived beating patterns are scattered in the high-efficiency zone predicted by the generic model. Furthermore, the flow rates and the transport efficiencies predicted by the generic kinematics are close to those obtained from experimental data, except for one data point, which differs from the generic model by a factor of about 2. These findings justify our choice of both the reduced design parameters and the generic model.

We now consider three-dimensional cilia kinematics and assess the effects of the out-of-plane swinging angle β_0 on $\langle Q\rangle$ and η. Namely, we vary β_0 from zero (results in Fig. 4) to 0.25π using increments of 0.01π. In Fig. 5 the values of $\langle Q\rangle$

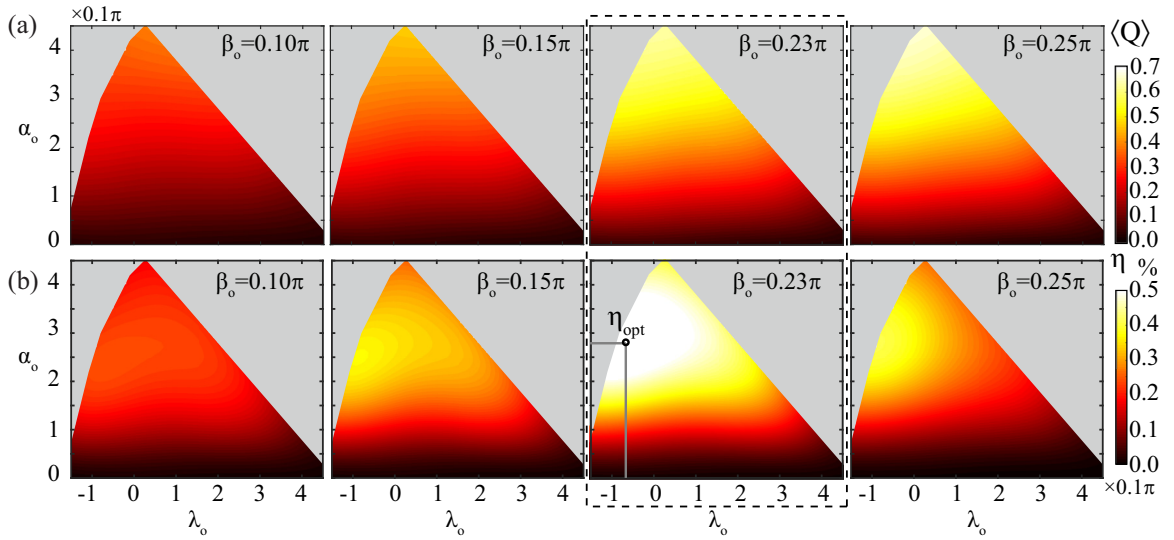

FIG. 5. (a) Average flow rates $\langle Q\rangle$ of generic cilia kinematics with different beating amplitude α_0, leaning angle λ_0, and swinging angle β_0. (b) Transport efficiencies.

and η are depicted for select values of β_0. Figure 5(a) shows that a larger swinging angle β_0 leads to a larger average flow rate. This is similar to the effect of the beating amplitude α_0 on the flow rate: The largest values of α_0 and β_0 ($\alpha_0 = 0.45\pi$ and $\beta_0 = 0.25\pi$) yield the largest average flow rate. The efficiency, on the other hand, is not a monotonically increasing function of β_0. Figure 5(b) shows that the efficiencies for $\beta_0 = 0.23\pi$ are higher than those for $\beta_0 = 0.25\pi$ at the same values of λ_0 and α_0. In fact, we chose to depict the panels for $\beta_0 = 0.23$ because it is the out-of-plane angle that leads to maximum transport efficiency for $\lambda_0 = \lambda_{\rm opt} = -0.07\pi$ and $\alpha_0 = \alpha_{\rm opt} = 0.28\pi$. The maximum efficiency value is 0.56%.

To study the sensitivity of the cilia performance with respect to the design parameters λ_0, α_0, and β_0, we perturb each one of these parameters away from the optimal or most efficient combination while keeping the other two parameters the same. In particular, we set $\lambda_0 = \lambda_{\rm opt} + \Delta$, $\alpha_0 = \alpha_{\rm opt} - \Delta$, and $\beta_0 = \beta_{\rm opt} - \Delta$, where $(\lambda_{\rm opt}, \alpha_{\rm opt}, \beta_{\rm opt})$ is the optimal parameter combination that leads to the most efficient cilium. The most efficient beating pattern and the beating patterns perturbed from the most efficient one are shown in Fig. 6.

We introduce two measures of sensitivity: (i) a global sensitivity that evaluates the net change in flow transport $|\langle Q\rangle - \langle Q_{\rm opt}\rangle|/\langle Q_{\rm opt}\rangle$ and (ii) a local sensitivity that evaluates the rate of change in flow transport normalized by $\langle Q_{\rm opt}\rangle$. Here, by rates of change in flow transport we mean $|\partial\langle Q\rangle/\partial\lambda_0|$, $|\partial\langle Q\rangle/\partial\alpha_0|$, and $|\partial\langle Q\rangle/\partial\beta_0|$. Similarly, the net change in efficiency $|\eta - \eta_{\rm opt}|/\eta_{\rm opt}$ and rates of change of efficiency $|\partial\eta/\partial\lambda_0|$, $|\partial\eta/\partial\alpha_0|$, and $|\partial\eta/\partial\beta_0|$ are, respectively, global and local measures of the sensitivity in cilia efficiency as the beating kinematics deviate from that of the most efficient cilium. A lower sensitivity implies more robustness to perturbations imposed on cilia design parameters and vice versa.

In Fig. 7(a) is a depiction of the global sensitivities of both the transport flow rate and efficiency as a function of the deviation Δ from the optimal cilium kinematics. Both the flow rate and efficiency are more sensitive to the beating amplitude α_0 and out-of-plane swinging amplitude β_0 than to the leaning angle λ_0. For example, a perturbation $\Delta = 0.1\pi$ [dashed gray lines in Fig. 7(a)] in the swinging angle β_0 will reduce the flow rate by over 36%, as compared to a reduction of 25% and 3% when varying the beating amplitude α_0 and leaning angle λ_0 by the same amount, respectively. A similar trend is observed for the sensitivity in the transport efficiency η. The local sensitivity measures,

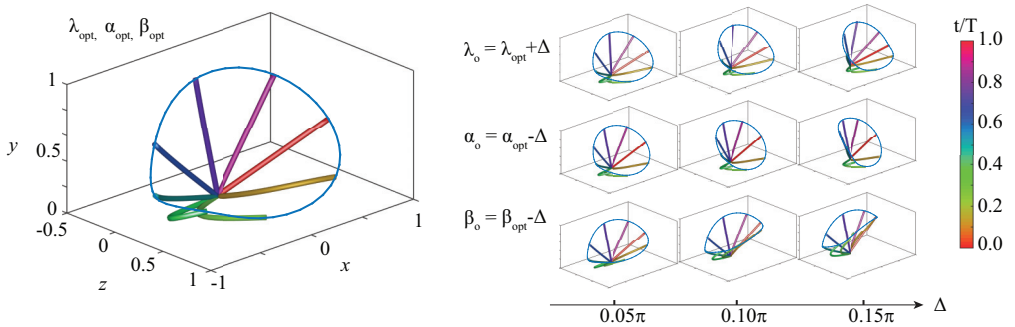

FIG. 6. Optimal (left) and suboptimal (right) beating patterns. The suboptimal beating patterns are constructed by perturbing one of the three design parameters while keeping the other two the same as in the optimal beating pattern.

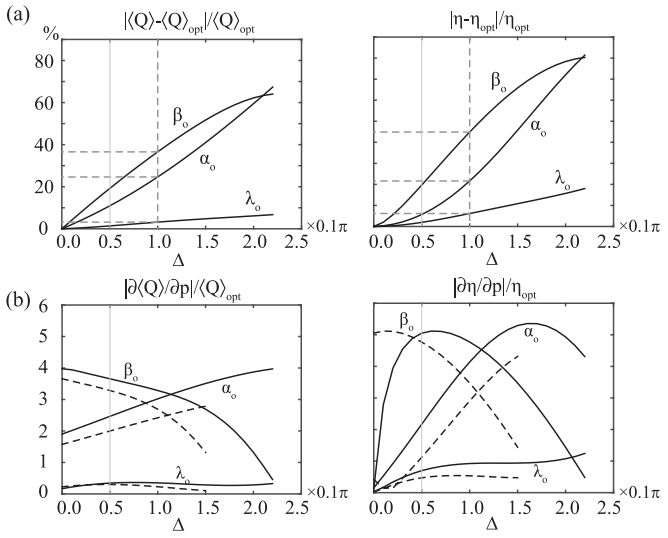

FIG. 7. Sensitivity of the net flow rate $\langle Q\rangle$ and the transport efficiency η with respect to perturbations Δ away from the optimal design parameters α_{opt}, λ_{opt}, and β_{opt}. (a) Global sensitivities or net change in $\langle Q\rangle$ and η as a function of Δ. (b) Local sensitivities or rate of change in $\langle Q\rangle$ and η as a function of perturbations Δ away from optimal parameter values (solid lines) and away from suboptimal parameter values (dashed lines).

shown in Fig. 7(b), confirm these findings, but indicate that for larger deviations from the optimal kinematics, the performance of the cilium becomes more sensitive to variations in beating amplitude α_0. These results indicate that to maintain lower sensitivity at large perturbations away from the optimal beating kinematics, a better strategy is to allow deviations in β_0 while restricting the variations in α_0. In other words, ciliary defects that induce large variations in α_0 lead to ineffective flow transport.

Figure 7(b) also shows the sensitivities associated with a suboptimal choice of cilia design parameters (dashed lines). Namely, instead of perturbing the parameters from λ_{opt}, α_{opt}, and β_{opt}, we consider the suboptimal parameters λ_{opt}, α_{opt}, and β^*, where $\beta^* = \beta_{\text{opt}} - 0.05\pi$ and impose perturbations Δ away from this suboptimal choice. Our goal is to compare the sensitivity of optimal and suboptimal design: The design with lower sensitivity is more robust to perturbations. It is evident from Fig. 7(b) that the local sensitivities of the flow rate and efficiency associated with the suboptimal design are lower than those associated with the optimal design for almost all Δ, indicating that a suboptimal design may lead to more robust performance when the design parameters are perturbed. Note that the only sensitivity component that is increased with this suboptimal choice of parameters is the sensitivity of transport efficiency with respect to the out-of-plane angle β_0 when the perturbation Δ is very small $\Delta < 0.04\pi$.

Finally, we set $\Delta = 0.05\pi$ (highlighted in light gray in Fig. 7) and we calculate the global and local sensitivities in transport efficiency η for all admissible values of λ_0 and α_0 for $\beta_0 = \beta^* = \beta_{\text{opt}} - \Delta$. In particular, we let λ^* and α^* denote the parameters that lead the highest transport efficiency η^* for $\beta_0 = \beta^*$ and we measure the global and local sensitivities relative to η^*. The results are depicted in Figs. 8(a) and 8(b), respectively. In the latter, the local sensitivities with respect to the design parameters α_0, λ_0, and β_0 are consolidated into one scalar function $(|\nabla\eta| - |\nabla\eta^*|)/\eta^*$, where $\nabla\eta$ is defined as $\nabla\eta = \sqrt{(\partial\eta/\partial\lambda_0)^2 + (\partial\eta/\partial\alpha_0)^2 + (\partial\eta/\partial\beta_0)^2}$. Such a depiction serves as a tool to identify the design parameters α_0 and λ_0 that satisfy desired limits on sensitivity given a perturbation size, in this case $\Delta = 0.05\pi$. For example, to ensure minimum sensitivities and maximum robustness for this perturbation size, one would choose values of α_0 and λ_0 that lie in the intersection of the regions that correspond to minimal sensitivities in Figs. 8(a) and 8(b).

A few comments on the interplay between efficiency and robustness are in order. At optimal efficiency, one has $\nabla\eta = 0$ by definition, which implies infinite robustness. However, cilia are often subject to perturbations in the fluid environment as well as in the ciliary apparatus. However, any perturbation away from the optimal beating pattern causes the cilium to lose efficiency. It is thus reasonable to assume that cilia often operate at suboptimal efficiency. The question then is, starting from suboptimal efficiency, how cilia transport is affected by further perturbations to the cilia beating kinematics. Interestingly, we found that starting from suboptimal efficiency, cilia transport may be more robust to perturbations than starting from optimal efficiency, hence, the most efficient cilium is not the most robust.

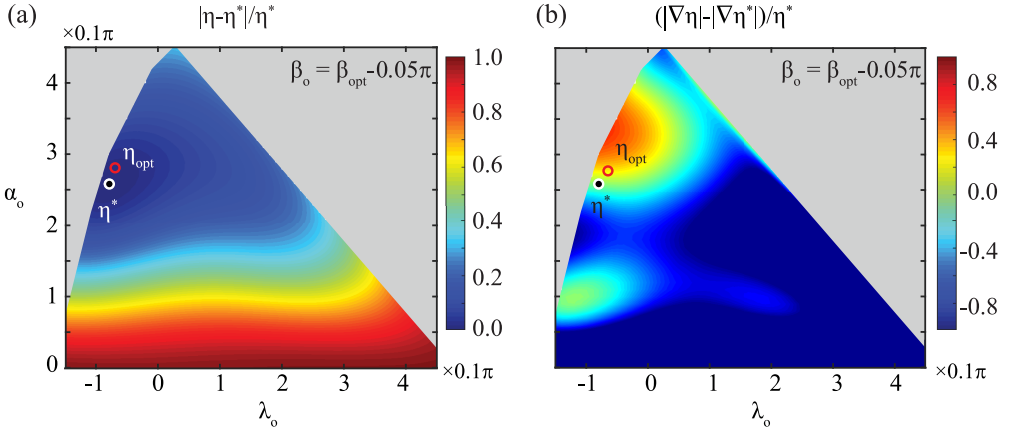

FIG. 8. (a) Global and (b) local sensitivities of the transport efficiency measured from a suboptimal choice of β^* as functions of λ_0 and α_0 for $\Delta = 0.05\pi$.

IV. CONCLUSION

We parametrized cilia beating kinematics using three reduced design parameters: the leaning angle λ_0 of the cilium in the direction of the effective stroke, the cilium beating amplitude α_0, and its out-of-plane swinging angle β_0. We presented a straightforward method for extracting these three parameters from experimental data. We also introduced a mathematical approach based on a sinusoidal family of time-dependent traveling waves that generate generic cilialike kinematics with prescribed values of λ_0, α_0, and β_0. To examine the performance of the various cilia kinematics, those obtained from experimental image sequences and those generated mathematically, we used two performance metrics: the net flow transported by the cilium and its efficiency.

We compared the performance of the generic cilialike kinematics (Fig. 3) with those reconstructed from experiments (Fig. 1). We restricted this comparison to the case of planar beating cilia due to the lack of experimental data that accurately resolve the out-of-plane cilia beating kinematics. In the planar case, one has only two design parameters: the leaning angle λ_0 and beating amplitude α_0. The flow rates and the transport efficiencies predicted by the generic kinematics are of the same order of magnitude as those obtained from experimental data (Fig. 4). Further, the design parameters extracted from the experimental data are all located in the region of the parameter space where the transport efficiencies are highest. Together, these observations provide strong evidence that both the reduced design parameters and the generic cilialike kinematics proposed in this work capture the salient features of cilia beating patterns.

We then presented a systematic study of the two performance metrics as a function of λ_0, α_0, and β_0 in the context of the generic cilia model. Our results suggest that the flow rates are positively affected by the beating amplitude α_0 and the out-of-plane swinging angle β_0 in the sense that larger values of α_0 and/or β_0 generate larger flow rates (Fig. 5). Indeed, both parameters amplify the asymmetry between the effective and recovery stroke, thus enhancing flow transport. Meanwhile, the transport efficiency is maximum for an optimal set of parameter values. Values α_0 and β_0 larger than these optimal values result in the cilium moving closer to the no-slip base surface. Since larger internal power is needed to move the cilium closer to the no-slip surface, such values lead to lower transport efficiency.

Finally, we examined the sensitivity of the flow rate and efficiency with respect to the design parameters. We investigated by how much the flow rate and efficiency would change as the design parameters deviate from the most efficient parameters. We called this a global sensitivity. We also examined a local sensitivity to parameter changes by computing how fast the transport flow rate and efficiency would change when perturbed away from the most efficient cilium. Our results show that perturbations in the out-of-plane angle β_0 or beating amplitude α_0 induce large sensitivities, that is, a deterioration in ciliary performance, whereas a change of the leaning angle λ_0 has no notable effect on the cilia performance (Fig. 7). Table I summarizes and compares the perturbation size needed in each of the design parameters to induce a 10% drop in the ciliary performance.

TABLE I. Perturbations of the design parameters (λ_0, α_0, and β_0) that lead to a 10% drop in the net flow rates and transport efficiencies relative to the optimal values.

Design parameter	$\langle Q \rangle$	η
λ_0		0.12π
α_0	0.05π	0.06π
β_0	0.03π	0.03π

Most importantly, our sensitivity analysis shows that the most efficient cilium is not most robust to perturbations in the cilia kinematics. Indeed, we presented a counterexample showing suboptimal parameters that are more robust (less sensitive) to perturbations (Fig. 8). Our results have two major implications. First, they confirm that designing for the most efficient cilium does not automatically impose any guarantees on robustness. It is our view that from the standpoint of evolutionary biology, robustness of design to natural or acquired variations is as important as efficiency itself. Therefore, when using genetic computational algorithms to compute ciliary design [18,19], one has to explicitly account for robustness. Second, our methods and results provide a quantitative framework for comparing the performance of cilia from different cell type, as well as cilia from the same cell type under different operating conditions such as in healthy and diseased states. To this end, one can begin to investigate quantitatively how perturbations and/or disruptions of the ciliary apparatus, whether due to a genetic disorder or infective and acquired causes, affect the flow transport. Low and inefficient flow rates of ciliated surfaces in mammalian organisms are directly linked to infection and disease, such as in cystic fibrosis and asthma. A quantitative map from cilia parameters to flow rates and vice versa would therefore provide an important tool for assessing cilia performance in health and disease.

ACKNOWLEDGMENT

Computation for the work described in this paper was supported by the University of Southern California's Center for High-Performance Computing [37].

[1] P. Satir and S. T. Christensen, Annu. Rev. Physiol. **69**, 377 (2007).
[2] G. R. Fulford and J. R. Blake, J. Theor. Biol. **121**, 381 (1986).
[3] C. O'Callaghan, K. Sikand, and A. Rutman, Pediatr. Res. **46**, 704 (1999).
[4] S. H. Randell and R. C. Boucher, Am. J. Resp. Cell Mol. Biol. **35**, 20 (2006).
[5] M. R. Del Bigio, Glia **14**, 1 (1995).
[6] Z. Mirzadeh, Y.-G. Han, M. Soriano-Navarro, J. M. García-Verdugo, and A. Alvarez-Buylla, J. Neurosci. **30**, 2600 (2010).
[7] R. Lyons, E. Saridogan, and O. Djahanbakhch, Hum. Reprod. Update **12**, 363 (2006).
[8] L. Wong, I. F. Miller, and D. B. Yeates, J. Appl. Physiol. **75**, 458 (1993).

[9] A. Wanner, M. Salathé, and T. G. O'Riordan, Am. J. Resp. Crit. Care Med. **154**, 1868 (1996).
[10] J. R. Davenport and B. K. Yoder, Am. J. Physiol.—Renal **289**, F1159 (2005).
[11] S. K. Chopra, G. V. Taplin, D. H. Simmons, and D. Elam, CHEST J. **71**, 155 (1977).
[12] D. Smith, E. Gaffney, and J. Blake, Resp. Physiol. Neurobiol. **163**, 178 (2008).
[13] D. Smith, E. Gaffney, and J. Blake, Proc. R. Soc. London Ser. A **465**, 2417 (2009).
[14] W.-E. Li, W. Chen, Y.-F. Ma, Q.-R. Tuo, X.-J. Luo, T. Zhang, W.-B. Sai, J. Liu, J. Shen, Z.-G. Liu *et al.*, Pflüg. Arch. Eur. J. Physiol. **464**, 671 (2012).
[15] Y. Ding, J. C. Nawroth, M. J. McFall-Ngai, and E. Kanso, J. Fluid Mech. **743**, 124 (2014).
[16] M. Fliegauf, T. Benzing, and H. Omran, Nat. Rev. Mol. Cell Biol. **8**, 880 (2007).
[17] B. Afzelius, J. Pathol. **204**, 470 (2004).
[18] C. Eloy and E. Lauga, Phys. Rev. Lett. **109**, 038101 (2012).
[19] N. Osterman and A. Vilfan, Proc. Natl. Acad. Sci. USA **108**, 15727 (2011).
[20] H. Guo, J. Nawroth, Y. Ding, and E. Kanso, Phys. Fluids **26**, 091901 (2014).
[21] V. A. Tucker, Comp. Biochem. Physiol. **34**, 841 (1970).
[22] Y. Katsu-Kimura, F. Nakaya, S. A. Baba, and Y. Mogami, J. Exp. Biol. **212**, 1819 (2009).
[23] M. A. Sleigh, Symp. Soc. Exp. Biol. **22**, 131 (1968).
[24] G. I. Taylor, Proc. R. Soc. London Ser. A **209**, 447 (1951).
[25] D. Eshel and C. J. Brokaw, Cell Motil. Cytoskel. **7**, 160 (1987).
[26] P. V. Bayly, B. L. Lewis, P. S. Kemp, R. B. Pless, and S. K. Dutcher, Cytoskeleton **67**, 56 (2010).
[27] P. Sartori, V. Geyer, A. Scholich, F. Jülicher, and J. Howard, arXiv:1511.04270.
[28] R. Cortez, L. Fauci, and A. Medovikov, Phys. Fluids **17**, 031504 (2005).
[29] J. Ainley, S. Durkin, R. Embid, P. Boindala, and R. Cortez, J. Comput. Phys. **227**, 4600 (2008).
[30] N. Liron, J. Fluid Mech. **86**, 705 (2006).
[31] D. J. Smith, J. R. Blake, and E. A. Gaffney, J. R. Soc. Interface **5**, 567 (2008).
[32] K. Machin, J. Exp. Biol **35**, 796 (1958).
[33] C. Brennen and H. Winet, Annu. Rev. Fluid Mech. **9**, 339 (1977).
[34] M. Hines and J. J. Blum, Biophys. J. **41**, 67 (1983).
[35] F. Gittes, B. Mickey, J. Nettleton, and J. Howard, J. Cell Biol. **120**, 923 (1993).
[36] E. Lauga and T. R. Powers, Rep. Prog. Phys. **72**, 096601 (2009).
[37] http://hpcc.usc.edu